



Original Research

# Zn containing mesoporous bioglasses with enhanced textural and antibacterial properties produced by three modifications of the sol-gel method

Anastasia Beketova<sup>1,2</sup> · Georgia K. Pouroutzidou<sup>3</sup> · Eleana Kontonasaki<sup>3</sup> · Veronica Giourieva<sup>4,5</sup> · Krisjanis Smits<sup>1,2</sup> · Valentina Stepanova<sup>1,2</sup> · Ioannis Tsamesidis<sup>3</sup> · Rajan Choudhary<sup>6</sup> · Kristaps Rubenis<sup>1,2</sup> · Toms Valdemars Eiduks<sup>7</sup> · Maria Bousnaki<sup>3</sup> · Dagnija Loca<sup>1,2</sup> · Rigini Papi<sup>4</sup> · Athanasia Pylostomou<sup>1,2</sup> · Janis Locs<sup>1,2</sup>

Received: 18 May 2025 / Accepted: 21 October 2025

© The Author(s) 2025

## Abstract

Mesoporous bioactive glasses (MBGs) have potential applications in bone tissue regeneration around tooth implant and local drug delivery. Small amounts of zinc added to their composition could additionally provide antibacterial and osteoinductive and anti-inflammatory properties. In this study, zinc-containing mesoporous bioactive glasses (5ZnO–25CaO–70SiO<sub>2</sub>) were synthesised using three modified surfactant-assisted sol-gel methods: dilute water (MZ1), Stöber (MZ2), and microemulsion-assisted (MZ3). X-ray diffraction (XRD) analysis confirmed that MZ1 and MZ3 were amorphous, while MZ2 exhibited a ZnO crystalline phase. The synthesised particles showed uniform morphology with sizes ranging from 10 to 500 nm. Brunauer–Emmett–Teller (BET) analysis revealed that MZ1 had the highest specific surface area (726 m<sup>2</sup>/g), approximately 4.1 times higher than MZ3 (176 m<sup>2</sup>/g). Haemolysis testing showed that MZ1 and MZ2 were non-haemolytic, whereas MZ3 caused lysis of erythrocytes. All samples were biocompatible with periodontal ligament fibroblasts, maintaining cell viability above 80% after three days of incubation. Antibacterial assays indicated that MZ2 exhibited over 60% inhibition of *P. intermedia* in a dose-dependent manner, but only ~20% inhibition of *P. gingivalis*. MZ2 demonstrated a bacteriostatic effect and was most effective in reducing anaerobic bacterial populations among all tested groups. These results highlight the potential of Zn-containing mesoporous bioactive glasses as multifunctional biomaterials for periodontal tissue engineering, suitable for such applications as scaffolds, bone cements, bone-filling granules, and antibacterial implant coatings. Furthermore, MZ2 material due to its antimicrobial properties, can potentially be a material of choice in periodontitis/peri-implantitis therapy applications.

✉ Anastasia Beketova  
anastasiabeketova@yahoo.com

✉ Janis Locs  
janis.locs@rtu.lv

<sup>1</sup> Institute of Biomaterials and Bioengineering, Faculty of Natural Sciences and Technology, Riga Technical University, Paula Valdena Street 3 k-1, LV-1048 Riga, Latvia

<sup>2</sup> Baltic Biomaterials Centre of Excellence, Headquarters at Riga Technical University, Riga, Latvia

<sup>3</sup> Department of Prosthodontics, Faculty of Health Sciences, School of Dentistry, Aristotle University of Thessaloniki, Thessaloniki GR-54124, Greece

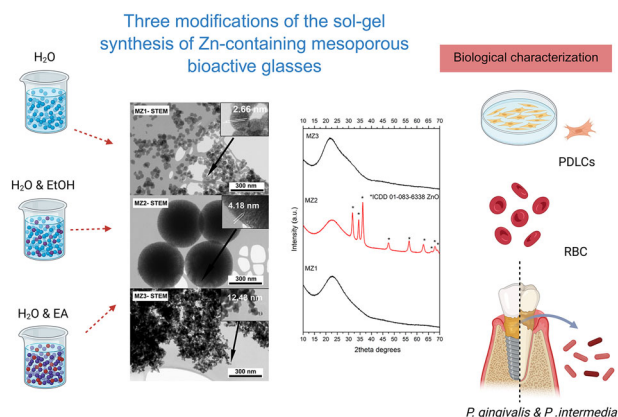
<sup>4</sup> Laboratory of Biochemistry, Department of Chemistry, Aristotle University of Thessaloniki, 54124 Thessaloniki, Greece

<sup>5</sup> Department of Botany, School of Biology, Aristotle University of Thessaloniki, 54124 Thessaloniki, Greece

<sup>6</sup> School of Chemistry, University College Dublin, Belfield, Dublin 4, Ireland

<sup>7</sup> Institute of Materials and Surface Technologies, Riga Technical University, P. Valdena str. 7, LV-1048 Riga, Latvia

## Graphical Abstract



## 1 Introduction

Antibiotic resistance has become a global challenge, according to the World Health Organisation. Every year, at least 700,000 people worldwide pass away from infections caused by resistant bacteria [1]. A reason for that is the prolonged use and overuse of antibiotics and implantation of medical devices, which might form a bacterial biofilm on their surface, becoming a source of chronic infection [2]. Recently, an increase of antibiotic resistance in patients with infection around tooth implants (peri-implantitis) was reported [3]. Peri-implantitis is a biofilm-induced infection caused by anaerobic oral microflora, such as *P. gingivalis* and *P. intermedia*. These bacteria are also responsible for such symptoms as gum bleeding, implant mobility and oral malodour. In 56% of cases, this infection leads to implant failure [4]. Considering that the dissemination of oral pathogenic bacteria might implicate cardiovascular diseases [5], there is a strong need to develop alternative antibacterial therapeutic approaches to eliminate antibiotic-resistant oral pathogens.

One of the novel strategies to prevent colonisation of the resistant Gram-negative anaerobic bacteria on the implant surface is the application of antibacterial bioactive glasses in situ to achieve a bacteria-free environment for re-osseointegration [2]. Bioactive glasses are widely used as bone grafting materials in dentistry (e.g. Perioglas®, Novabone®) due to their osteoconductive and osteoinductive properties [6, 7]. In the last two decades, nanoscale bioactive glasses with mesoporous ordered structure evolved as the latest generation of smart multifunctional materials. Mesoporous bioactive glasses (MBGs) have been proposed as bioactive fillers and drug carriers either alone or combined with other materials, taking advantage of their unique porous structure to load drugs, biomolecules and antibacterial ions [8] MBGs are produced by addition of

structure-directing agents into sol-gel chemistry, so that they acquire a large pore volume, a highly organised structure of channel-like pores in the 2–50 nm range, and a large specific surface area (600–1500 m<sup>2</sup>) [9, 10]. MBGs in the binary system SiO<sub>2</sub>-CaO exhibit better apatite-forming capacity, and superior biological properties, as compared to non-mesoporous sol-gel or melt-derived bioactive glasses (BGs) [11]. Their enhanced texture facilitates quick ion exchange between the glass surface and the surrounding biological media, leading to fast supersaturation and precipitation of surface hydroxyapatite. Furthermore, nano-dimensional features of mesoporous glasses favour their direct interactions with cells and components of extracellular matrix.

MBGs can incorporate different active metal ions like Zn, Ag, Cu, Ce, Ga to boost their antibacterial properties [6, 11–13]. These antibacterial MBGs can prevent biofilm formation and induce bacteria-free environment for rapid healing. The mechanism behind their antibacterial action could be explained by rapid therapeutic ion release, and local changes of pH. The unique surface characteristics of MBGs could additionally provide non-specific action against bacterial membrane. In contrast to conventional metal oxide nanoparticles, such antibacterial glass formulations are non-toxic and biocompatible. Therefore, antibacterial MBGs seem promising materials for treatment of antibiotic-resistant peri-implant infection and promotion of de novo bone formation around tooth implant.

Among various antibacterial ions, zinc is known for its relative low toxicity and excellent antibacterial and anti-inflammatory properties. Zinc is a necessary trace element in the human body that comes from food sources. The total amount of zinc in the body is approximately 1.5 g in women and 2.5 g in men [14]. Zinc participates in cellular metabolism, including DNA and protein synthesis, cell signaling and division. 30% of Zn is accumulated in human

bones and it is actively involved in the synthesis of the collagen matrix, mineralisation, and bone remodelling [15]. Zinc also contributes to wound healing processes by promoting fibroblast and epithelial cell migration and proliferation [16]. Due to its antibacterial properties Zn is also formulated into many oral care products for control over plaque and calculus, as the main causes of periodontal disease [17]. In dentistry, zinc oxide eugenol cements are indicated for temporary tooth filling and indirect pulp capping in case of pulp inflammation. They relieve pain and elicit bacteriostatic and antiseptic action. Zinc has a major role in immune function regulation, bacterial infection control, inflammatory response balancing, and oxidative stress reduction—all of which are linked to the pathophysiology of periodontal disease [18]. Furthermore, the potential to inhibit biofilm formation of zinc-containing glasses has been reported recently [19].

Mesoporous bioactive glasses are typically produced by the sol-gel method with addition of pore-forming agents. Sol-gel technique has numerous advantages such as low processing temperatures, simplicity and possibility to tailor the materials for a specific application. In the most commonly used Stöber modification, a cationic surfactant cetyl trimethylammonium bromide, or CTAB, can be added to the synthesis solution to guide the formation of mesopores [20]. A silicate precursor tetraethyl orthosilicate (TEOS) and metal ion precursors are usually added into the water/ethanol solution under basic conditions and carefully stirred. Then, the resulting nanoparticles are filtered, dried and calcined to form mesoporous nanoparticles. The Stöber technique may produce uniform MBG spheres, which typically have diameters between 100 and 400 nm [21]. By adjusting molar ratios, pH and added precursors it is possible to create a variety of nanoparticles with diverse morphologies and sizes. In the microemulsion assisted sol-gel process, organic molecules, such as ethyl acetate can also be added during the synthesis to achieve a more uniform shape of the particles or to increase their dispersity. Unfortunately, using traditional sol-gel based methods to synthesise highly dispersed MBGs with multiple metallic ions remains difficult because metallic precursors can weaken the stability of nanoparticles during synthesis, which leads to aggregation and irregularity in the final MBGs.

To date, only a few studies exist regarding Zn-doped MBGs (Zn-MBGs). Nešćáková et al. synthesised highly dispersed Zn-containing MBGs in the CaO-SiO<sub>2</sub> system using an emulsion assisted sol-gel method [22]. However, they had a relatively low specific surface area, and their antibacterial properties were not investigated. Another study reported that the extract of Zn-doped binary SiO<sub>2</sub>-CaO MBGs received after incubation in culture medium at a concentration of 0.1 mg/mL exhibited anti-inflammatory

properties and promoted the osteogenic capacity of rat bone marrow stromal cells (BMSCs) [23]. Naruphontjirakul et al. used strontium (Sr)- and zinc (Zn) to partially substitute calcium and synthesised MBG nanoparticles (MBGNs) in the binary system SiO<sub>2</sub>-CaO using an emulsion assisted sol gel method and tested the antibacterial activity using the disc diffusion method against *E. coli* and *S. aureus* [24]. They found statistically significant increase in antibacterial effect against Gram-negative bacteria (*E. coli*). Pourshahrestani et al. applied the same method for doping MBG with Zn with molar contents of 1, 2 and 4% as substitutes of either calcium and silicon and observed a slight decrease of bacterial viability of *S. aureus* and *E. coli* at the highest concentrations of their extracts [25].

In another attempt, zinc-doped bioactive glass porous nanoparticles in the system 60SiO<sub>2</sub>-30CaO-5ZnO-5P<sub>2</sub>O<sub>5</sub> (mol%) were, developed and incorporated into alginate/chitosan composite hydrogel as a wound dressing [26]. The authors observed efficient antibacterial effect against *E. coli* and *S. aureus* and wound healing in an in vivo rat model.

Summarising the aforementioned reports, all the Zn-MBGs were synthesised by the emulsion assisted sol-gel method, and exhibited promising antibacterial, osteogenic, and anti-inflammatory properties, although issues regarding the optimisation of their composition and improvement of antibacterial effectiveness are still open for further research, to fully explore their clinical potential. There are almost no reports on the use of the modified Stöber synthesis method to produce such materials, while there are no available data on the antibacterial properties Zn-doped MBGs with oral pathogens, that would exploit their potential as therapeutic agents in the treatment of peri-implantitis and periodontitis.

The aim of this study was to synthesise Zn containing MBGs (5ZnO-25CaO-70SiO<sub>2</sub>%mol) using three different modifications of the surfactant-assisted sol-gel method: (a) modified Stöber method under dilute water conditions [27, 28] (b) modified Stöber method with addition of ethanol as a solvent [29] and (c) the microemulsion-assisted sol-gel approach [30], and to compare their hemocompatibility, biocompatibility and antibacterial properties against anaerobic bacteria related to periodontitis and peri-implantitis.

## 2 Materials and methods

### 2.1 Synthesis of Zn-containing mesoporous bioactive glasses

The reactants that were used for the synthesis: sodium hydroxide (NaOH), ammonium hydroxide 25%, hexadecyltrimethylammonium bromide (CTAB), tetraethyl orthosilicate (TEOS), ethyl acetate, Ca(NO<sub>3</sub>)<sub>2</sub>·4H<sub>2</sub>O,

$\text{Zn}(\text{NO}_3)_2 \cdot 6\text{H}_2\text{O}$  were purchased from Sigma-Aldrich (now Merck KGaA, Darmstadt, Germany).

Three types of Zn-containing mesoporous bioactive glasses (Zn-MBGs) with the nominal composition  $70\text{SiO}_2\text{--}25\text{CaO}\text{--}5\text{ZnO}$  (mol%) were synthesised using three modifications of the surfactant-assisted sol-gel method described in the literature.

MZ1 powder was synthesised using modified sol-gel method using water as a solvent. Initially, CTAB, a soft template for the mesoporous structure, was dissolved in the basic aqueous medium (pH=12), followed by the addition of TEOS as a source of Si and nitrate salts as a source of Ca and Zn metal ions. In detail, 0.315 g NaOH was dissolved in 785 ml of ultrapure water to achieve an alkaline medium (pH=12), where 1 gram of CTAB was dissolved. Then, 7.5 ml of TEOS were added to the mixture dropwise. After 30 min, the appropriate quantity of calcium nitrate tetrahydrate was added and mixed for 8 h at the  $T = 80^\circ\text{C}$ , followed by the addition of zinc nitrate hexahydrate and mixing for additional 1.5 h at the same temperature. The precipitate after washing was dried at  $60^\circ\text{C}$  for 24 h and calcined at  $550^\circ\text{C}$  for 5 h with a heating rate of  $1^\circ\text{C}/\text{min}$  to remove the templating agent and nitrates.

MZ2 material was produced by a modification of the sol-gel method with addition of ethanol as a solvent at room temperature [29]. The first step involved dissolving 1 g of the surfactant CTAB in the mixture of 150 ml of ultrapure water, 30 ml of ethanol, and 2 ml of ammonium hydroxide, which served as a catalyst. Following CTAB dissolution, the appropriate amounts of  $\text{Ca}(\text{NO}_3)_2 \cdot 4\text{H}_2\text{O}$  and  $\text{Zn}(\text{NO}_3)_2 \cdot 6\text{H}_2\text{O}$  were added simultaneously to the mixture and continuously stirred for 30 min. After that, 7.5 ml of TEOS was added dropwise and the resulting solution was stirred for additional 4 h. Then, the white precipitates were filtered and washed twice with distilled water. Samples were then dried for 24 h at  $60^\circ\text{C}$ . Lastly, they were calcined at  $550^\circ\text{C}$  for 5 h with a heating rate of  $1^\circ\text{C}/\text{min}$ .

For the synthesis of MZ3 material the micro-emulsion assisted sol-gel method of the protocol of Neščáková et al. was strictly followed [22]. In brief, 2.24 g of CTAB was dissolved in 104 mL of ultrapure water for 30 min at  $30^\circ\text{C}$ . 32 ml of ethyl acetate was then gradually added to the mixture while it was continuously stirred for additional 30 min. To keep the pH at 10.5 after that, ammonium hydroxide (28%) was added. Following that, 23.04 mL of TEOS was added and agitated for 30 min. Further, 4.34 g of calcium nitrate tetrahydrate and 1.09 g zinc nitrate hexahydrate were added with interval of 30 min and continuously stirred for additional 4 h. The suspension was centrifuged and washed twice with ultrapure water. Finally, the precipitate was dried in an oven at  $60^\circ\text{C}$  for 24 h, and calcinated at  $700^\circ\text{C}$  for 2 h at a heating rate of  $2^\circ\text{C}/\text{min}$ .

## 2.2 Physicochemical characterisation

### 2.2.1 Fourier Transform Infra-red Spectroscopy (FTIR-ATR)

A Fourier transform infra-red spectrometer (Thermo Scientific Nicolet<sup>TM</sup> iSTM50, Waltham, MA, USA) in Attenuated Total Reflectance (ATR) mode was used to evaluate the molecular structure of the produced powders. The FTIR absorption spectra were obtained in range of the wavelengths between 4000 and  $400\text{ cm}^{-1}$ , with 64 scans, and resolution of  $4\text{ cm}^{-1}$ . The OMNIC software was used for the data processing.

### 2.2.2 X-ray Diffraction (XRD)

X-ray powder diffractometry (PANalytical, Aeris, Netherlands) was used for crystalline phase analysis of the specimens. The X-ray source for the XRD apparatus was a copper (Cu) tube, which ran at 40 kV and 15 mA. The diffraction data were obtained within the range of  $10 - 70^\circ 2\theta$  with a step size of  $0.0435^\circ 2\theta$  degrees. Complementary analysis was performed with X'PertHighScore and the International Centre for Diffraction Data PDF-2 (ICDD) database, while ICDD card #01-083-6338 was used for ZnO identification.

### 2.2.3 Brunauer–Emmett–Teller (BET) and Brunauer–Joyner–Halenda (BJH) analysis

The specific surface area (SSA), and the volume and size of pores in the synthesised powders were analysed using a nitrogen gas adsorption/desorption system (Quadrascorb evo, Quantachrome instruments, Boynton, FL, United States) by Brunauer–Emmett–Taylor (BET) according to ISO standard 9277:2010 (E) and Brunauer–Joyner–Halenda (BJH) methods. Before analysis, the specimens were vacuum-degassed at ambient temperature for 24 h.

### 2.2.4 Scanning Electron Microscopy (SEM) with Energy Dispersive X-ray Analysis (EDX) and Scanning Transmission Electron Microscopy (STEM)

The surface morphology of the mesoporous materials was visualised by scanning electron microscope (Verios 5UC (Thermo Scientific, USA)). For SEM measurements, samples were secured using an electrically conductive double-sided adhesive carbon tape on standard aluminium pin stubs. Images were captured in vector scanning mode using a TLD SE detector with an acceleration voltage of 2 kV. Prior to SEM-EDS measurement, samples were sputter-coated with carbon using a Leica EM ACE200 sputter coater (Leica). An X-MAX 150 EDX (Oxford) analysis was performed to qualitatively investigate the sample

composition. The pore morphology, configuration and particle size of the synthesised Zn-MBGs were evaluated by STEM. For sample preparation a small amount of powder was dispersed in isopropyl alcohol and sonicated in an ultrasonic bath for 5 min. Further, the specimens were placed on a carbon coated grid and dried before analysis. For STEM measurements, samples were transferred to a holey carbon film 400 Cu mesh (AGS147-4). For STEM imaging, an STM3+ detector was used at 30 kV.

### 2.2.5 X-ray fluorescence spectroscopy (XRF)

Qualitative and semiquantative bulk analysis of the specimens was performed on a Rigaku supermini, sr.no. 16019-3 XRF wavelength dispersive spectrometer equipped with an Pd tube, with three analysing crystals: LiF1 (for elements Ti-U), PET (for elements Al-Ti), RX25 (for elements F-Mg). The detectors were a SC scintillation counter, set up with LiF1 crystal for Ti-U and F-PC flow proportional counter, set up with PET and RX25 for F-Ti. Samples were analysed at 50 kV and 4 mA tube-operating conditions, F-U element range with step sizes: 0.02 deg (Ti-U), 0.05 (F-Ca) and scanning speed 15 deg/min. Sample spin was turned on, making the sample cup rotate during measurement.

## 2.3 Bioactivity evaluation

For the evaluation of the in vitro bioactivity, the synthesised materials were immersed into Simulated Body Fluid (SBF) solution prepared according to Kokubo et al.'s protocol for 21 days [31]. All specimens, equal in volume, were placed into sterile, clean bottles and incubated in SBF at a concentration of 75 mg/50 mL at 37 °C under static conditions. Filtration was used to extract the powdered samples from the SBF, which were subsequently cleaned with ultrapure water and dried for 24 h at 60 °C. XRD, FTIR and SEM-EDS were employed to analyse the materials for calcium-phosphate or apatite crystals formation.

## 2.4 In vitro biological properties evaluation

### 2.4.1 Haemolysis assay

For the haemolysis assay, whole blood was taken from healthy adults after their written consent. Red blood cells (RBCs) were isolated from leucocytes and plasma by centrifugation for 5 min at a speed of 2000 rpm and washed three times using phosphate buffered saline (PBS). A final suspension of 2% RBCs volume was obtained by diluting RBCs in PBS (2% haematocrit). After that, red blood cells were mixed separately with various MBGs concentrations (0.06, 0.125, 0.5, and 1 mg/ml) derived from a stock solution (5 mg/mL) and incubated for 24 h at 37 °C. The

untreated red blood cells' supernatant (Ctrl-) served as the negative control, while the red blood cells treated with lysis buffer served as the positive control. After the treated RBCs were centrifuged at 2000 rpm for one minute, the supernatants were collected and analysed using a microplate reader (Epock, Biotek Instruments, Inc., Winooski, Vermont, USA). The absorbance of the released haemoglobin was measured at 541 nm, with a reference wavelength of 700 nm. The percentage of haemolysis was calculated based on three independent trials using the following equation:

$$\text{Hemolysis\%} = \frac{[\text{sample absorbance} - \text{negative control}]}{[\text{positive control} - \text{negative control}]} \times 100$$

### 2.4.2 In vitro cytocompatibility assay

Primary cell culture of periodontal ligament fibroblasts (PDLFs) was established from periodontal ligament tissue received from a healthy young donor after extraction of his third molars and signing the informed consent form. The potential cytotoxicity of the synthesised MBGs was assessed in direct contact with PDLFs using the MTT (3-(4,5-dimethylthiazol-2-yl)-2,5-diphenyltetrazolium bromide) assay. Initially, 96 well plates were seeded with  $10^3$  cells each in DMEM culture medium (Dulbecco Modified Eagle's medium- Biosera, Nuaille, France) supplemented with 10% FBS serum (Foetal bovine serum 10%, Gibco-BRL, Thermo Fisher Scientific Inc., Waltham, Massachusetts, USA) and antibiotics/antimycotics (penicillin, amphotericin B, streptomycin (Gibco-BRL, Thermo Fisher Scientific Inc., Waltham, MA, USA)). The cells were left for 24 h to adhere in an incubator with 5% CO<sub>2</sub> atmosphere at 37 °C. Then, MBGs were precisely weighted and sterilised with UV light for 30 min. 1 mg/ml stock solutions of MBGs were prepared and precultured in a culturing medium for 24 h. Further, a sequence of dilutions with nanoparticles at two concentrations (0.25 and 0.5 mg/mL) were added to well-plates and cell viability was evaluated after 24 and 72 h of incubation. Cells that were not in contact with the materials were used as the positive control. To determine the mitochondrial dehydrogenase activity of living cells, Dimethyl sulfoxide (DMSO) was added (Sigma Aldrich, St. Louis, MO, USA), to dissolve purple formazan crystals. Using the microplate reader measurements were performed at the wavelength of 570 nm, with a 630 nm reference filter. Tests were conducted in quintuplicate. The outcomes were given as a percentage of the control average optical density. For all the in vitro biocompatibility a statistical t-test and one-way analysis of variance (ANOVA) were performed via the use of the GraphPad Prism 8.4.2 software programme, and the significance level was determined at  $p < 0.05$ .



## 2.5 Evaluation of the antibacterial properties

### 2.5.1 Bacteria preparation

The antibacterial activity of powders was investigated using the *Prevotella intermedia* (DSM 20706) and *Porphyromonas gingivalis* (DSM 20709). Strains were grown in modified peptone yeast glucose (PYG) medium for 3–4 days under anaerobic conditions (80% N<sub>2</sub>, 10% H<sub>2</sub>, 10% CO<sub>2</sub>) and agitation (130 rpm) at 37 °C. Bacterial stocks were kept as frozen glycerol aliquots in –80 °C. The Gas-Pak EZ Gas Generating Pouch Systems (BD, Benex Limited, Dublin, Ireland) were used to generate the anaerobic environment for both antibacterial evaluation in liquid broth dilution assay and in agar plate dilution methods.

### 2.5.2 Liquid broth dilution assay

For the liquid broth dilution assay, fully grown anaerobic bacteria were incubated in the presence of the materials for 3 days at 37 °C, at 130 rpm and under anaerobic conditions. At first, materials were sterilised under UV lamp for 20 min, sonicated for dispersion in PYG medium in water bath for 20 min at 37 °C and subjected to serial dilutions. Bacterial growth was evaluated by optical density (OD<sub>600nm</sub>) using the JENWAY 6305 spectrophotometer. Fully grown bacterial cultures were used to prepare the 10% (v/v) suspension (corresponding to 10<sup>8</sup> cfu/ml) in PYG medium for each strain that was added to the materials suspensions at the concentrations 0.125, 0.25, 0.5, 1 and 2 mg/ml. Bacterial growth was determined by measuring the optical absorption OD<sub>600nm</sub> at 600 nm. Control growth (medium without inoculum) and blanks (medium with tested materials) were also evaluated. The % absorbance was determined as the absorbance ratio of material treated bacteria suspension to fully grown suspension (control). Means and standard deviations were calculated to evaluate tendency and variability for each condition.

### 2.5.3 Colony forming unit CFU assay

The antibacterial activity of MZ1, MZ2 and MZ3 were evaluated by spread agar plate CFU (colony forming unit) counting. The treated and untreated bacterial culture was serially diluted and 25 µL spread in anaerobe CDC blood agar plates (Bioprepure) and grown at 37 °C under anaerobic conditions for 2 days. Colonies were counted and inhibitory activity was determined by the following equation:

$$\% \text{inhibition} = (\log_{10} \text{CFU}_{\text{control}} - \log_{10} \text{CFU}_{\text{treated}}) * 100 / \log_{10} \text{CFU}_{\text{control}}$$

where, CFU<sub>control</sub>: number of colonies from non-treated specimens, CFU<sub>treated</sub>: number of colonies in contact with

materials. All experiments were performed under anaerobic conditions with two replicates.

## 3 Results

### 3.1 FTIR

The FTIR spectra of all three Zn containing MBGs show the distinctive bands of amorphous silicate glasses [32]. (Fig. 1a) In particular, the band at 800 cm<sup>-1</sup> is ascribed as Si–O–Si bending vibration, while the band at 470 cm<sup>-1</sup> is assigned to the Si–O–Si rocking vibration. The IR spectra also revealed a broad band between 1000 and 1250 cm<sup>-1</sup> that was made up of the transverse optical mode (TO1) of the Si–O–Si stretching vibration at 1090 cm<sup>-1</sup> and a shoulder at 1220 cm<sup>-1</sup> that was ascribed to the TO2 mode [33]. Additionally, there is a shoulder at about 960 cm<sup>-1</sup> in materials MZ1 and M2, which is associated with the Si–OH bonds' stretching vibration [33]. However, no discernible alterations, that might be attributed to the presence of ZnO phase were detected on FTIR spectra. The main absorption band for the Si–O–Zn bond (stretching vibration) is located around 457 cm<sup>-1</sup> [34] or 474 cm<sup>-1</sup> [35], which is probably overlapped with the Si–O–Si (rocking) vibration, located at 470 cm<sup>-1</sup>.

### 3.2 XRD

The powders MZ1, MZ2 and MZ3 had a typical XRD pattern (Fig. 1b) of amorphous silicate materials, with a characteristic scattering pattern at around 2θ = 18–28° which corresponded to amorphous silicates [36]. MZ2 material also contained ZnO crystalline phase with characteristic diffraction peaks located at 2θ degrees = ~31.7, 34.4, 36.2, 47.3, 56.6, 62.7, 62.9, 66.4, 67.7, 69.1 °2θ that can be assigned to hexagonal ZnO. (ICDD card #01–083–6338).

### 3.3 BET/BJH analysis

The N<sub>2</sub> adsorption-desorption isotherms of MZ1, MZ2 and MZ3 powders are presented in Fig. 2. MZ1, MZ2, and MZ3 are classified as mesoporous silica nanoparticles. These nanomaterials show isotherms resembling Type IV in their nitrogen adsorption-desorption isotherms. In addition, it appears that MZ1 has a definite hysteresis loop, most probably of the H1 type, which indicates that it has large cylindrical mesopores containing a significant volume of adsorbed substance and is highly porous. The MZ2 sample, on the other hand, not only contains considerable inter-particle pore space, but also has a larger hysteresis loop that represents a blend of orderly and irregular mesopores with a wider range of pore sizes (H1/H2 type). Between MZ1 and

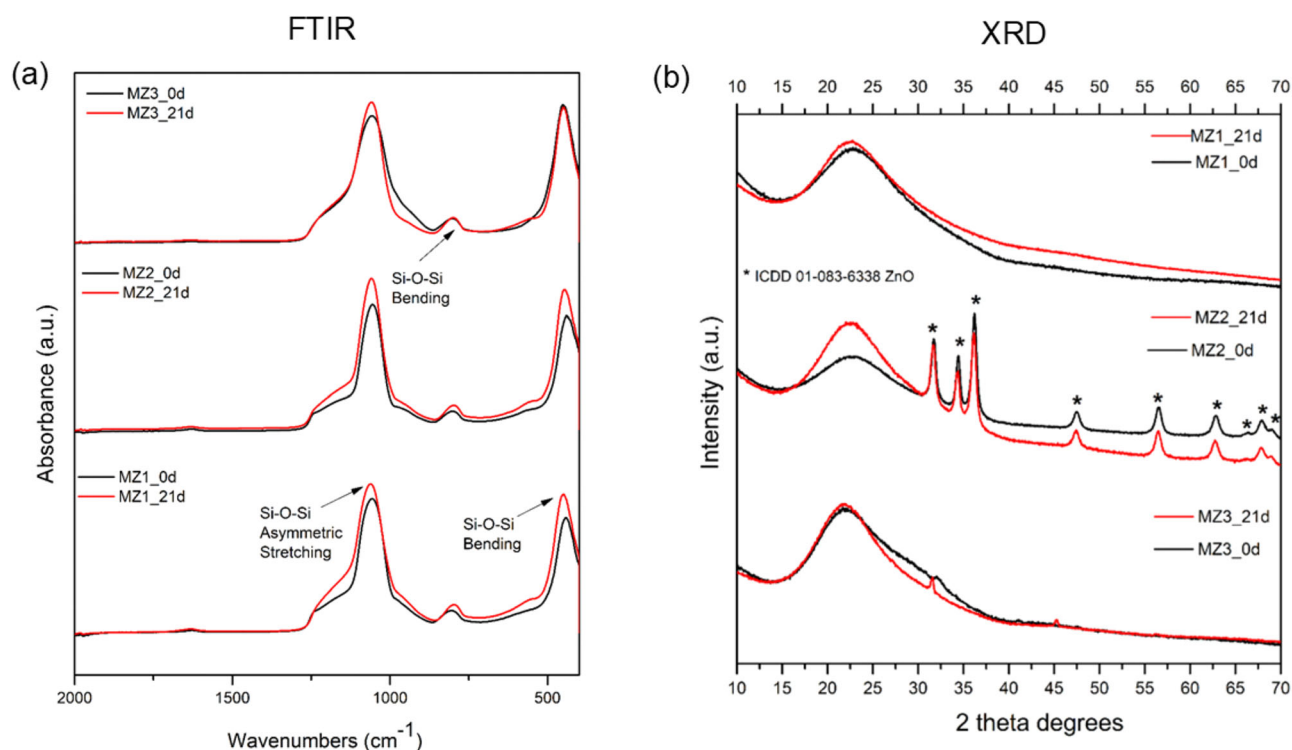


**Fig. 1** **a** FTIR spectra of the synthesised powders, initial spectra and after 21 days in SBF **b** XRD analysis of the Zn-MBGs before and after immersion to SBF

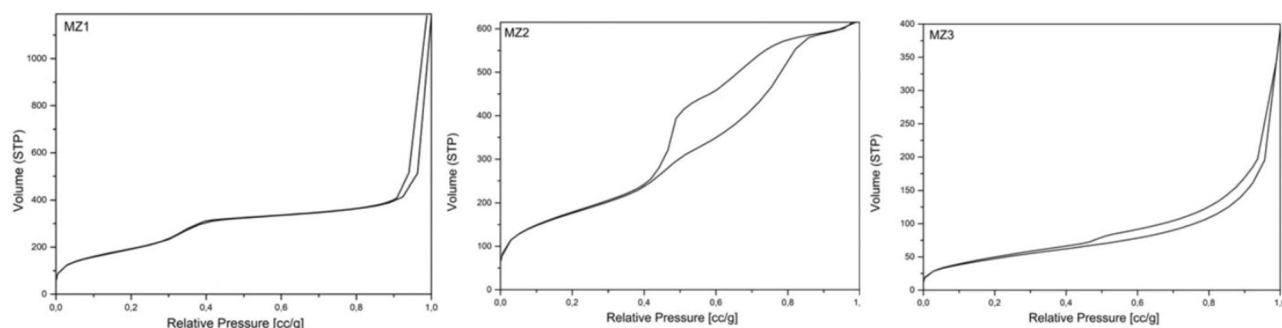


**Fig. 2** N<sub>2</sub> adsorption-desorption isotherms of MZ1, MZ2 and MZ3 powders

MZ2 on one side and MZ3 on the other, there appears to be a gradual increase in the pore structure's homogeneity since the latter has a finer hysteresis loop relative to the two former samples. Especially in connection with their clear differences in pore structure and adsorption behaviour, the latter view explains the reason why these materials could be applicable for drug delivery systems, catalysis processes and adsorption techniques. Surface characteristics of the MZ1, MZ2 and MZ3 powders according to BET/BJH analysis are depicted in Table 1.

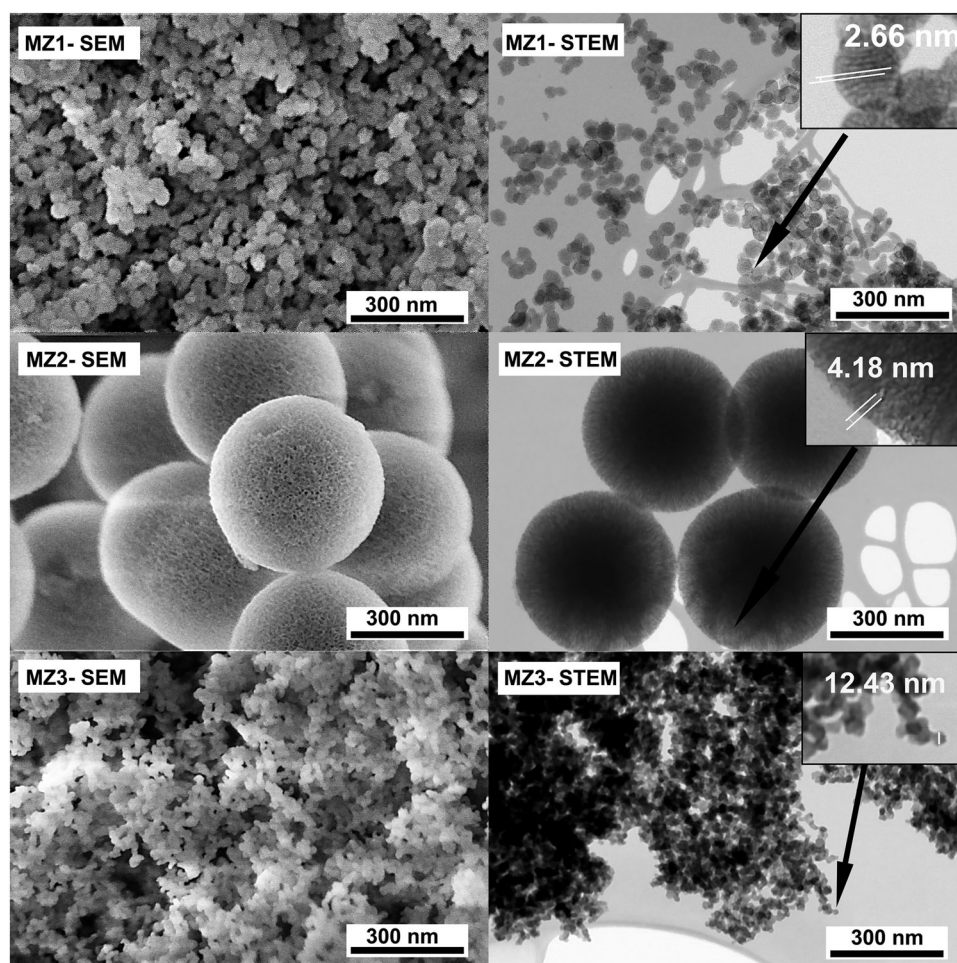
### 3.4 SEM/EDS and STEM analysis

The morphology of the prepared particles was analysed by scanning electron microscopy (SEM) and STEM, that

**Table 1** Surface characteristics of the MZ1, MZ2 and MZ3 powders according to BET/BJH analysis

Specimen	CTAB/TEOS ratio	Specific Surface area (SSA, $\text{m}^2/\text{g}$ )	Pore volume ( $\text{cm}^3/\text{g}$ )	BJH pore diameter (nm)
<b>MZ1</b>	1/7.5	726.9	1.54	2.97
<b>MZ2</b>	1/7.5	634.4	1.03	3.84
<b>MZ3</b>	1/10.28	176.1	0.57	3.88

were depicted on Fig. 3. MZ1 material shows homogeneous, slightly agglomerated particles with average size 30–50 nm. In MZ1 material hexagonal ordered mesoporous channels running parallel to one another are visible in the STEM pictures, suggesting that the

**Fig. 3** SEM/STEM images of the synthesised materials

distinctive mesoporous long period order has not been impacted by Zn ion doping. The powdered MZ2 exhibits apparent nano-porosity and dispersed, spherical particles with an average size of 450–550 nm. Alongside the mesoporous structure, STEM images also show spherical, fluffy particles with a rough surface and tiny void pores. According to SEM analysis MZ3 powder appears non-homogenous with different forms of mesoporous agglomerates and ultra small particles of an average size of few nanometres. In STEM images, the material presented loose agglomerates consisting of 10–13 nm rounded particles.

### 3.5 XRF

The chemical composition of all Zn-MBGs, observed by XRF is presented in the Table 2. By comparing the nominal and detected composition, a limited incorporation of calcium ions can be noted, especially in the specimen MZ1 (1.87%). MZ1 powder had the highest molar percent of ZnO (9.63%), while the lowest content of ZnO was in MZ3 powder (3.63%).

**Table 2** Chemical compositions (mass %) of Zn-MBGs determined from the XRF results

	Nominal Composition	MZ1	MZ2	MZ3
<b>SiO<sub>2</sub></b>	70.0%	88.5%	89.44%	84.84%
<b>CaO</b>	25.0%	1.87%	2.63%	11.53%
<b>ZnO</b>	5.0%	9.63%	7.93%	3.63%
<b>Total</b>	100.0%	100.0%	100.0%	100.0%

### 3.6 Bioactivity evaluation

FTIR and XRD analysis revealed lack of alterations in specimens MZ1\_21 d and MZ2\_21 d in SBF, as compared to the initial materials (Fig. 1a, b). MZ3–21d material shows two additional crystalline diffraction peaks of low intensity at 31.5 and 45.2 2θ degrees, which we were not able to identify. SEM analysis showed no considerable surface changes in specimens MZ1 and MZ3 and obvious increase of surface roughness in material MZ2, attributed to dissolution-precipitation processes on its surface in SBF (Fig. 4). EDX analysis of the initial materials demonstrated



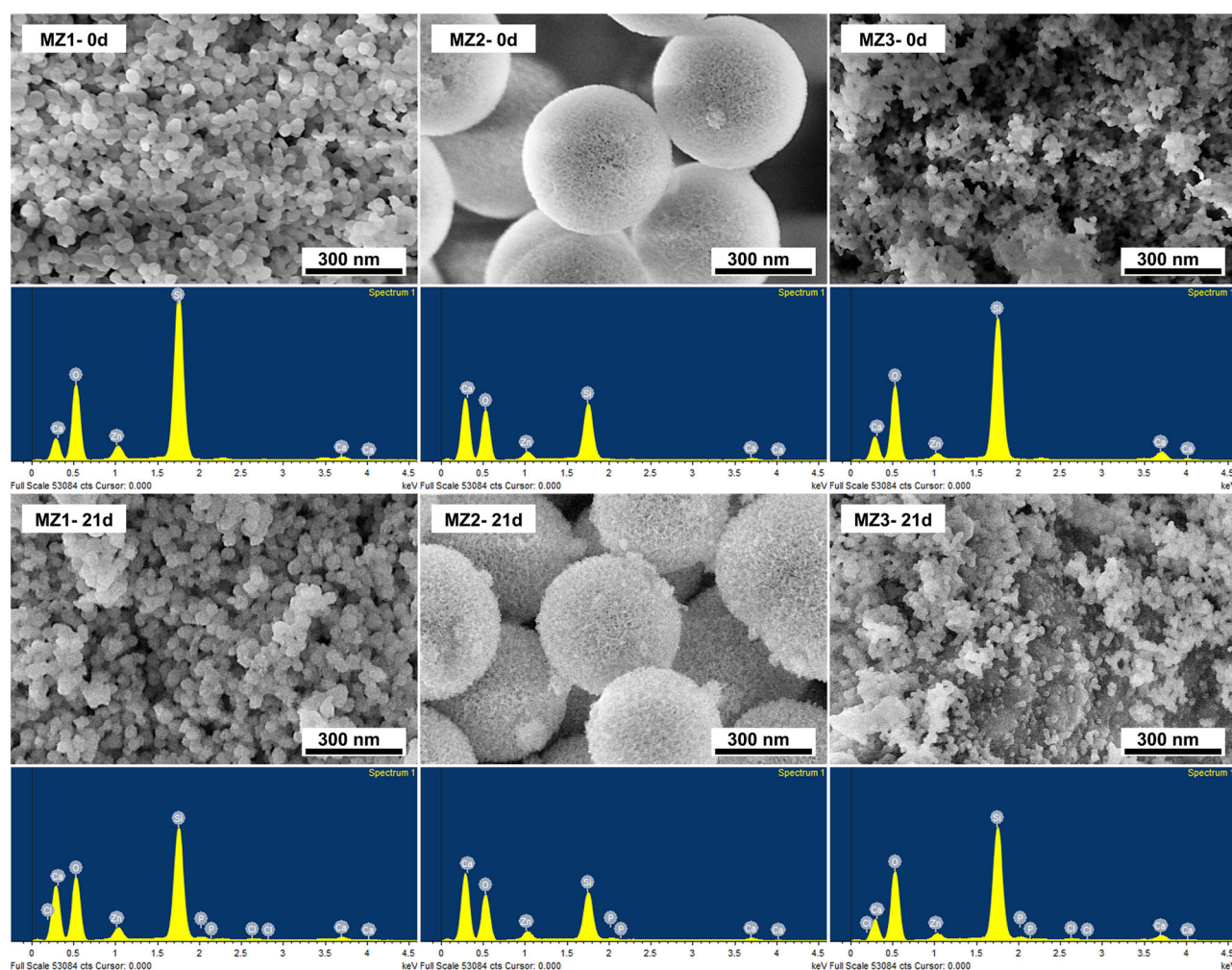


**Fig. 4** SEM-EDS analysis of the Zn-MBGs before and after immersion to SBF

the presence of calcium and zinc peaks in the corresponding spectra, indicating that these ions were successfully incorporated into the materials' structure (Fig. 4). EDX spectra of the specimens that were maintained in SBF for 21 days showed only small quantities of Ca, P, Cl and Na. (Fig. 4). Therefore, all three Zn-MBGs did not exhibit pronounced ability to form hydroxyapatite surface layer.

### 3.7 Haemolysis evaluation

Two of the tested materials MZ1 and MZ2 presented no haemolysis (<2%) at the tested concentrations, while MZ3 appeared to be haemolytic in a concentration-dependent manner (Fig. 5a).

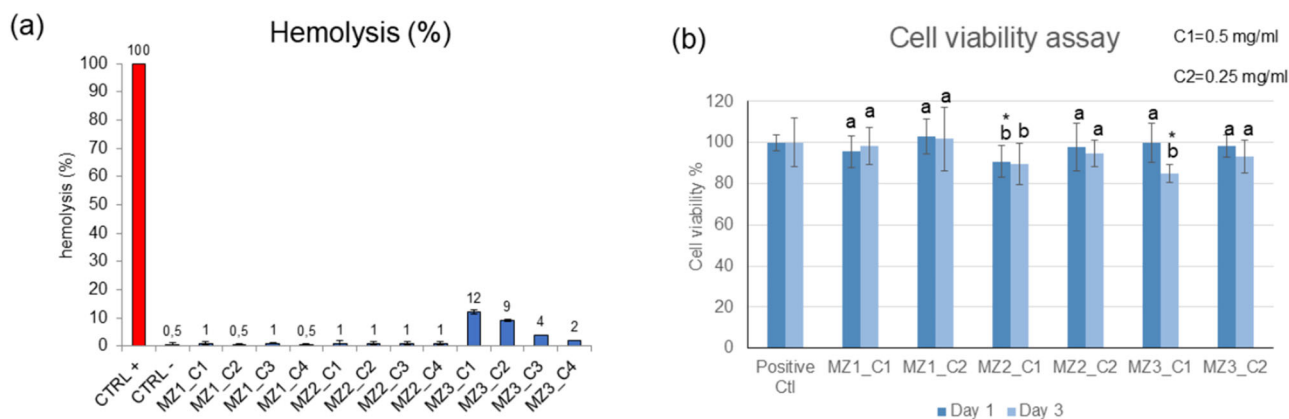
### 3.8 In vitro biocompatibility assay

Figure 5b presents relative cell viability (%) of PDLCs in contact with the tested materials. MZ1 specimens did not show any negative effect on the viability of PDLCs at both

tested concentrations of 0.25 mg/ml and 0.5 mg/ml, as compared to the control. MZ2\_C1 and MZ3\_C1 specimens caused a reproducible, statistically significant ( $p < 0.05$ ) reduction of cell viability/proliferation of 9.3% at 1<sup>st</sup> day and 15.2% at 3<sup>rd</sup> day, respectively, as compared to the control. Significant differences were observed between intergroups across both days and doses, with MZ2\_C1 and MZ3\_C1 showing consistently lower cell viability compared to other conditions, as indicated by distinct statistical groupings ( $p < 0.05$ ). No significant differences were detected between Day 1 and Day 3 within most groups, suggesting that the observed lower cell viability is primarily dose-dependent rather than time-dependent. However, all tested materials are considered biocompatible, as their viability was above 80% after 3 days of incubation with cells.

### 3.9 Antibacterial studies

Antibacterial activity of MZ1, MZ2 and MZ3 was evaluated using two methods: liquid broth dilution method



**Fig. 5** **a** Diagram representing the percentage of haemolysis of human RBCs upon incubation with Zn-MBGs at different concentrations (1 (C1), 0.5 (C2), 0.25 (C3), 0.06 (C4) mg/ml) at 37 °C after 24 h of incubation. **b** MTT cell viability assay of PDLs treated with various

concentrations of Zn-MBGs. The symbol \* represents the statistically significant difference, at  $p < 0.05$ , between each concentration and the control group. Different letters represent the statistically significant intergroup differences (concentrations and days)

### Broth dilution method

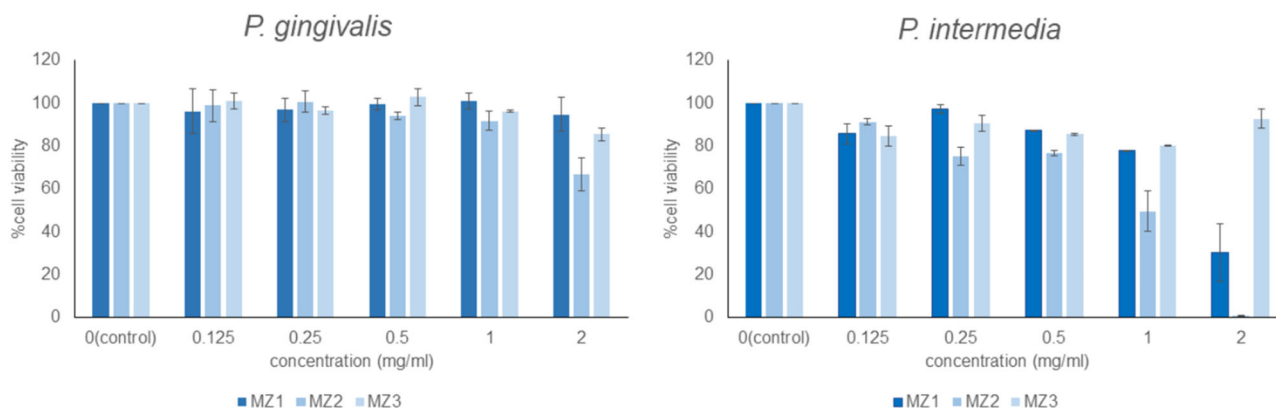


**Fig. 6** Investigation of antibacterial activity of Zn-MBGs with liquid broth dilution assay against *P. intermedia* and *P. gingivalis*. MZ2 has the most consistent and dose dependent antibacterial activity against both *P. gingivalis* and *P. intermedia*

[37] and CFU assay. From liquid broth dilution method MZ1 and MZ2 showed a dose dependent antibacterial activity against *P. intermedia*, while MZ3 had the lowest antibacterial activity at all concentrations. Particularly, MZ2 presented 1.32% cell viability at the concentration of 2 mg/ml, while MZ1 showed a 30.2% bacterial viability at the same concentration (Fig. 6). For *P. gingivalis* MZ2 material presented 66.8% of bacterial viability in comparison to the respective control group. Antibacterial activity of MZ2 was further verified by CFU assay. For MZ2 a 62% inhibition was observed at the concentration 2 mg/ml. Low bacterial inhibition was observed with MZ1 and MZ3 at all the tested concentrations (Fig. 7). For *P. gingivalis* MZ2 also showed the highest antibacterial activity among all materials according CFU assay, which however didn't exceed 18%.

## 4 Discussion

In this study, we synthesised three Zn containing mesoporous bioactive glass materials with the same molar compositions ( $5\text{ZnO}-25\text{CaO}-70\text{SiO}_2\%$ mol) using three modifications of the sol gel method, each with a unique obtained composition and structure. FTIR and XRD analysis revealed that MZ1 and MZ3 were mainly composed of an amorphous Si-O-Si network with homogeneous inclusion of Ca and Zn ions into the amorphous structure. On the other hand, in the MZ2 material a ZnO crystalline phase was formed. Limited zinc ion incorporation into the silica network and precipitation of ZnO crystalline phase in the material MZ2 can be attributed to the synthesis process due to late addition of TEOS, that followed after the addition of nitrate salts. ZnO nanocrystals could be possibly entrapped

## CFU assay

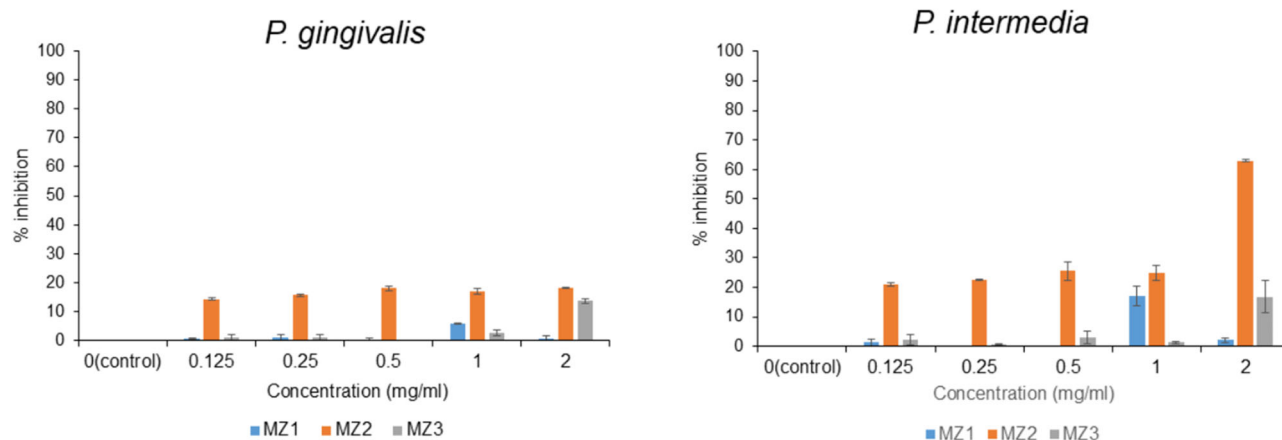


**Fig. 7** Determination of inhibitory activity of Zn-MBGs against *P. intermedia* and *P. gingivalis* by CFU assay. The CFU assay further verified the antibacterial activity of MZ2

inside the mesoporous structure or located within amorphous network of the MZ2 material.

According to XRF all synthesised MBGs showed notable compositional differences, with respect to the nominal composition. The highest molar percentage of CaO was observed in MZ3 material (11.53%), while MZ1 and MZ2 powder had the high content of ZnO (9.63% and 7.93%) and relatively low CaO percentage. This could be explained by the limited inclusion of Ca ion into amorphous silica network during sol-gel synthesis or its removal during the centrifugation and washing steps. The increased ZnO content as compared to the nominal composition in specimen MZ1 could be possibly attributed to the competitive incorporation of smaller ions  $\text{Zn}^{2+}$  instead of larger  $\text{Ca}^{2+}$  ions [38] into the glass structure [39]. This finding is in agreement with the lower CaO content.

The highest surface area (726.9  $\text{m}^2/\text{g}$ ) and highest pore volume (1.54  $\text{cm}^3/\text{g}$ ) were observed in the material MZ1, followed by MZ2 material, which is expected to facilitate protein adsorption or drug loading. In contrast, MZ3 material had the lowest specific surface area. Notably, the SSA and pore volume of MZ1 and MZ2 materials, obtained by two modified Stöber methods were 2–3 times higher than of similar materials produced by other techniques [22, 40, 41].

Application of different modifications of base-catalysed sol-gel process led to production of mesoporous nanoparticles with different shapes and sizes due to changing the essential synthesis parameters including pH, reaction duration, and temperature, as well as the addition of the organic molecules [20, 42]. The modified Stöber method under dilute water conditions to produce MZ1 material resulted in uniform 30–50 nm sized particles with narrow size distribution and well-defined periodic mesoporous structure.

Such small particle size could possibly be attributed to a high water/ TEOS ratio and addition of NaOH catalyst instead of ammonia that favours formation of shorter CTAB micelles [27]. Material MZ2 was synthesised using the classical Stöber process that resulted in the formation of large mesoporous spherical particles with sizes in the range of 450–550 nm. Silica precursor TEOS was hydrolysed in an ethanol-water mixture in the presence of ammonia as a catalyst. The Ca and Zn that were previously added in the ethanol–water solution, were partially incorporated into the silicon oxygen network to form BG sol nanoparticles. Then, the vast quantities of BG sol nanoparticles interacted with the rod-like CTAB micelles through electrostatic interaction, resulting in the formation of BG–CTAB complexes. To reduce the overall energy, the BG–CTAB complexes aggregated to form spherical structure in the ethanol–water solution under stirring [43, 44]. After calcination, CTAB was removed, and mesoporous bioactive glass spheres of 450–550 nm were obtained. The particle size depends on the rate of two processes, the hydrolysis that affects nucleation and TEOS condensation; lower hydrolysis rate and higher condensation rate results in large particles [34]. Large particles were produced as a result of ethanol's suppression of TEOS hydrolysis. The same is true for other alcohols like propanol and ethylene glycol, although propanol can produce particles as large as about 200 nm [45]. There are both synergistic and antagonistic interactions among the experimental variables (ethanol, water, TEOS, and ammonia concentrations), which also vary depending on their respective concentration ranges. A comprehensive multivariate study on the impact of reaction parameters on particle size could provide more insight into the proper combinations to control both size, Zn incorporation and dispersibility.

MZ3 material was synthesised by the emulsion assisted sol-gel process in accordance to the protocol of Nešćáková et al. [22] As it is commonly considered, this method allows the production of particles with uniform compositions and good dispersity, as well as the inclusion of metal ions. The size of MBGs could range from 28 nm to 250 nm [46], and by varying the proportion of aqueous ammonia utilised, they could acquire a spherical or pineal-like shape. In brief, in the presence of hydrophobic ethyl acetate (EA) molecules, the CTAB micelles will self-assemble with EA to form oil in water microemulsion droplets. The oil phases may serve as barriers that stop the nanoparticles from aggregating, while the surfactants stabilise the microemulsion droplets [12]. Specifically, MBG-Zn nanoparticles, synthesised by Nešćáková et al. had spherical (ovoidal) shape and size of about 130 nm, and they were well-dispersed. The particles, obtained in our study were of size of 10–13 nm and were mostly aggregated. Notably, the synthesis protocol of Nešćáková et al. differs in TEOS/ EA/ water ratios, as compared to classical protocol of Liang et al. [46], applied elsewhere, that might partially explain divergences in the obtained results.

For drug delivery applications controlling the size and shape of mesoporous bioactive glasses is crucial, as they directly affect their transport within body, their interactions with cells and, the kinetics of drug release [21]. In general, spherically shaped particles exhibit superior injectable and cohesive qualities and are preferred over irregularly shaped ones [21, 28]. Hydrodynamic stability in the bloodstream is achieved by keeping the drug carrier's particle size between 50 and 300 nm; particles smaller than this would tend to disperse non-specifically throughout the body because of microscopic intercellular gaps in the normal blood vessel walls, while particles larger than this would be entrapped in the liver and lungs [28].

The apatite forming ability of all three materials was tested through immersion to simulated body fluid with **ion concentrations** almost the same to those of **human blood plasma** [31]. The mechanism of bioactivity, according to Larry Hench [47], involves five sequential steps: glass dissolution, ionic exchange between the biological medium and the glass surface, repolymerization of surface's silica-rich layer, followed by precipitation of amorphous calcium phosphate, and its crystallising into carbonated hydroxyapatite (CHA) layer. As it was previously reported, silica-based mesoporous bioglasses form hydroxyapatite layer within only 1 day, due to quick dissolution and porous texture of these material [48]. In our study, all three materials containing Zn did not form hydroxyapatite even after 21 days of immersion to SBF solution, according to FTIR, XRD and SEM data. As reported, the addition of zinc into bioactive glass in concentration exceeding 5% has been shown to retard the formation of hydroxyapatite [41, 49, 50].

This can be attributed to several factors. First of all, in the bioactive glass structure, ZnO can function as an intermediate oxide or as a network modifier [51], reducing glass solubility. [52, 53]. Secondly,  $\text{Zn}^{2+}$  ions can be adsorbed on the active hydroxyapatite nucleation sites and substantially inhibit crystal growth [40]. In consistency with our findings, Nešćáková et al. reported that Zn-containing MBG was not bioactive after 14 days of soaking in SBF [22]. Notably, the intensity of ZnO patterns was decreased after SBF soaking in MZ2 material, which probably resulted from either the formation of the calcium phosphate amorphous precipitates on the surface of nanoparticles or some dissolution of the ZnO nanoparticles in the SBF medium [40].

The evaluation of hemocompatibility is essential for nanoparticles, which are intended to be used for drug delivery particularly via intravenous administration [54]. However, it is also important to test the haemolytic potential of any material, that will be implanted in the human body, especially when it is nano-dimensional. The haemolysis assay gives a clear notion of the adverse effects of nanoparticles that destroy red blood cells. RBC disintegration is associated with release of toxic forms of haemoglobin, which can cause oxidative stress and pro-inflammatory responses in tissues [55]. According to the ASTM standard (ASTMF-756-08, 2009) materials with in vitro haemolysis up to 2% are classified as non-haemolytic, while materials with haemolysis percentages between 2 and 5% are classified as moderately haemolytic. Only substances that cause haemolysis above the 5% threshold are categorised as haemolytic [56]. Numerous studies have demonstrated that haemolytic activity of mesoporous nanoparticles depends on concentration, their size and shape, surface area, porosity and surface charge, more importantly, on surface silanol content [57, 58]. Although there are quite controversial data in the literature regarding the impact of size on haemolytic activity, it is likely that smaller nanoparticles have higher haemolytic potential. We suppose that the haemolytic activity of MZ3 material could be attributed to its small particle size (~10 nm), that probably caused direct physical disrupting of RBCs membranes. In contrast, MZ1 and MZ2 materials presented no haemolysis at all the tested concentrations due to larger particle sizes, and, thus, it is expected that will not cause local inflammatory reactions in tissues, associated with lysis of RBCs.

MTT assay was performed in direct contact with PDLs. In vitro nanoparticle biocompatibility with specific cell lines depends on their physicochemical properties (chemical composition, size, shape, surface chemistry and charge), as well as the concentration of the nanoparticles, and the exposure time. All three materials were biocompatible, and showed cell viability above 80%. The MZ1 material showed the highest cell adhesion/proliferation rates, even though it



had the highest ZnO content among all the tested materials (9.63%). The majority of reports so far have concentrated on the cytocompatibility of glasses with low ZnO contents (3–8 mol.%). Cell culture studies with materials' extracts on mouse embryonic fibroblast cells (MEF), human dermal fibroblast (NHDF) cells showed no harmful effects on cells proliferation and even promoted differentiation of human osteoblast-like cells (MG-63, HOS) [22, 23, 25].

On the other hand, high quantities of zinc oxide (ZnO) in bioactive glasses have been shown to be harmful both in vitro and in vivo, although the exact mechanism of toxicity is still unknown. According to some research, the ZnO disintegrates to produce  $\text{Zn}^{2+}$ , which is more hazardous than ZnO nanoparticles. Cell death is the result of lysosomal and mitochondrial damage caused by the disruption of cellular Zn homeostasis after ZnO breakdown. The generation of reactive oxygen species (ROS) and the oxidative stress that follows could be another pathway. Adenosine triphosphate (ATP) depletion in cells may result from zinc's inhibition of important enzymes in the glycolytic process [2]. Thus, cytotoxic effects of MBG containing 20% ZnO for mesenchymal stem cells has been reported [24].

Antibacterial activity of Zn doped bioglasses is usually investigated in the context of hospital acquired diseases management as an alternative for antibiotic resistant microflora. Sanchez-Salcedo et al. reported antimicrobial activity against *St. aureus* and good biocompatibility of the scaffolds with 4 mol% ZnO addition [59]. Very good antimicrobial activity against *P. aeruginosa* and *B. subtilis* strains was achieved by Zn containing MBGs doped with 5% mole ZnO [41]. It is reported that Gram-positive bacteria are more susceptible to ZnO. These are in accordance with the findings of Sergi et al. who did not observe any inhibitory effect of ZnO included bioactive glasses (2, 3.8, and 5 mol%) against the Gram-negative species *E. coli* and *P. aeruginosa*, but found out dose-dependent antibacterial behaviour against *S. epidermis* [60].

To effectively treat peri-implantitis and periodontal disease it is essential to eliminate polymicrobial communities of subgingival biofilms, that become pathogenic when key bacterial species like *P. gingivalis* and *P. intermedia* are present, creating a protective, matrix-embedded network that is immune system-resistant and resistant to antimicrobial agents. Recently, Esfahanizadeh et al. have investigated the efficacy of Zn containing sol-gel derived BG in improving the antibacterial properties against periodontal pathogens. The authors reported weak biofilm formation for Zn/BG through measuring the optical density (OD) at 570 nm wavelengths, while BG formed a partially adhered biofilm layer on the surface [19].

In this study we utilised two complementary methods to evaluate antibacterial activity: liquid broth dilution method and CFU assay. Liquid broth dilution method provides quantitative data for the antibacterial activity of the tested materials, guiding the effective treatment dose in the clinical setting. Moreover, the applied media contained all the necessary components for bacteria growth, to further resemble to the clinical conditions MZ2 material showed the highest antibacterial activity among all the tested groups, mostly against *P. intermedia*. This might be attributed to the presence of ZnO nanocrystals in its composition. According to some theories, ZnO may have antibacterial properties through breaking down the membrane of the bacterial cell, producing intercellular reactive oxygen species (like  $\text{H}_2\text{O}_2$ ) that can interact with bacterial cells and causing a marked increase in reactive oxygen species (ROS) in the bacterial cytoplasm [60]. However, in anaerobic conditions the exact mechanism of antibacterial action remains unclear.

Nanoparticle-based approaches in treatment of periodontitis and peri-implantitis could potentially solve the problem of bacterial resistance and simultaneously promote periodontal tissue regeneration and osteogenic repair. For instance, metal oxide nanoparticles ( $\text{Ag}_2\text{O}$ , CuO, ZnO,  $\text{Ti}_2\text{O}$ , etc.) exhibit strong non-specific action against bacterial membrane, however their cytotoxicity and toxic accumulation in cells, are the limitations for their further clinical translation [61]. Significant advantages of Zn-MBGs obtained in our study is their reduced cytotoxicity, as compared to ZnO nanoparticles [62], and their drug-loading capacity. As reported, Zn doped BGs also can be used as complementary strategy to reduce the doses of antibiotics. Using formulation  $80\text{SiO}_2\text{-}15\text{CaO}5\text{P}_2\text{O}_5$  (mol%), Heras et al. loaded two types of mesoporous bioactive glass scaffolds (undoped and 4% ZnO doped) with four distinct antibiotics: levofloxacin, vancomycin, gentamicin, and rifampicin. Studies on bacteria in vitro, showed that zinc ions and antibiotics worked synergistically against *S. aureus* and *E. coli* [63].

In this way, ZnO containing MZ2 material, synthesised by the modified Stöber method with ethanol addition could be a material of choice for periodontal therapies as an alternative to conventional antibiotics. e.g. as component of antibacterial gels applied locally after dental root/implant surface decontamination. Furthermore, it could be a promising biomaterial for periodontal tissue engineering in preparation of scaffolds, bone filling granules, bone cements and antibacterial implant coatings. Further research on its combination with other antibacterial substances, its osteogenic potential, and antibacterial action against other resistant pathogens will be needed to expand their application for orthopaedics and orofacial surgery.

## 5 Conclusions

In this study, we synthesised three Zn containing mesoporous bioactive glass materials with the same nominal molar compositions using three modifications of the sol-gel method. MZ1 and MZ3 materials were fully amorphous, while MZ2 material contained nano ZnO crystallised within the amorphous network. Particles' size ranged from approximately 10 nm to 550 nm. MZ1 and MZ2 materials, produced by two modifications of modified Stöber method exhibited enhanced surface characteristics with large surface area (726.9 m<sup>2</sup>/g and 634.4 m<sup>2</sup>/g) and pore volume, exceeding 2–3 times analogous materials reported in literature. Addition of ZnO suppressed bioactivity of all the specimens, while cell culture studies with PDLs showed that all the materials were cytocompatible. Their different physicochemical characteristics had an impact on their hemocompatibility-MZ1 and MZ2 materials were haemocompatible, while MZ3 caused lysis of erythrocytes. MZ1 material due to small size (~50 nm), spherical shape and hemocompatibility could be potentially utilised for intravenous drug delivery, taking advantage of its unique porous structure to load drugs, biomolecules and growth factors. Novel MZ2 material showed increased antibacterial activity against *P. intermedia* that could be ascribed to the presence of crystalline zinc oxide. In conclusion, among the ones investigated MZ2 has a favourable combination of properties which is worth additional investigation, e.g. in vivo tests, for potential use in regenerative dentistry.

**Acknowledgements** The research has been funded by RegrOssBio (HORIZON-MSCA-2022-PF-01-01) GA 101106882 project (financed by European Union). The authors also acknowledge the access to the infrastructure and expertise of the Baltic Biomaterials Centre of Excellence (BBCE, GA No. 857287).



**Funded by  
the European Union**

## Compliance with ethical standards

**Conflict of interest** The authors declare no competing interests.

**Publisher's note** Springer Nature remains neutral with regard to jurisdictional claims in published maps and institutional affiliations.

**Open Access** This article is licensed under a Creative Commons Attribution-NonCommercial-NoDerivatives 4.0 International License, which permits any non-commercial use, sharing, distribution and reproduction in any medium or format, as long as you give appropriate credit to the original author(s) and the source, provide a link to the Creative Commons licence, and indicate if you modified the licensed material. You do not have permission under this licence to share adapted material derived from this article or parts of it. The images or other third party material in this article are included in the article's Creative Commons licence, unless indicated otherwise in a credit line

to the material. If material is not included in the article's Creative Commons licence and your intended use is not permitted by statutory regulation or exceeds the permitted use, you will need to obtain permission directly from the copyright holder. To view a copy of this licence, visit <http://creativecommons.org/licenses/by-nc-nd/4.0/>.

## References

1. Mancuso G, Midiri A, Gerace E, Biondo C. Bacterial Antibiotic Resistance: The Most Critical Pathogens. *Pathogens*, 2021;10:1310. <https://doi.org/10.3390/pathogens10101310>.
2. Elahpour N, Niesner I, Abdellaoui N, Holzapfel BM, Gritsch L, Jallot E, et al. Antibacterial Therapeutic Ions Incorporation into Bioactive Glasses as a Winning Strategy against Antibiotic Resistance. *Adv Mater Interfaces*, 2024;11:2400068. <https://doi.org/10.1002/admi.202400068>.
3. Ardila CM, Vivares-Builes AM. Antibiotic Resistance in Patients with Peri-Implantitis: A Systematic Scoping Review. *Int J Environ Res Public Health*, 2022;19:15609. <https://doi.org/10.3390/ijerph192315609>.
4. Smeets R, Henningsen A, Jung O, Heiland M, Hammächer C, Stein JM. Definition, etiology, prevention and treatment of peri-implantitis - a review. *Head Face Med*. 2014;10:1–13. <https://doi.org/10.1186/1746-160X-10-34>.
5. Hofer AM, Dadarlat-Pop A, Mester A, Nasui BA, Popa M, Picos A. The impact of peri-implant diseases on the general status of patients with cardiovascular diseases: a literature review. *Life*. 2024;14:1–10. <https://doi.org/10.3390/life14060665>.
6. Zheng K, Kang J, Rutkowski B, Gawęda M, Zhang J, Wang Y, et al. Toward highly dispersed mesoporous bioactive glass nanoparticles with high Cu concentration using Cu/ascorbic acid complex as precursor. *Front Chem*, 2019;7:497. <https://doi.org/10.3389/fchem.2019.00497>.
7. Shearer A, Montazerian M, Sly JJ, Hill RG, Mauro JC. Acta Biomaterialia Trends and perspectives on the commercialization of bioactive glasses. *Acta Biomater*. 2023;160:14–31. <https://doi.org/10.1016/j.actbio.2023.02.020>.
8. Tang F, Li L, Chen D. Mesoporous Silica Nanoparticles: Synthesis, Biocompatibility and Drug Delivery. *Adv Mater*, 2012;24:1504–1534. <https://doi.org/10.1002/adma.201104763>.
9. Liverani L, Boccardi E, Beltran AM, Boccaccini AR. Incorporation of calcium containing mesoporous (MCM-41-type) particles in electrospun PCL fibers by using benign solvents. *Polymers*. 2017;9:1–16. <https://doi.org/10.3390/polym9100487>.
10. Yan X, Yu C, Zhou X, Tang J, Zhao D. Highly ordered mesoporous bioactive glasses with superior in vitro bone-forming bioactivities. *Angew Chem Int Ed*. 2004;43:5980–5984. <https://doi.org/10.1002/anie.200460598>.
11. Zheng K, Sui B, Ilyas K, Boccaccini AR. Porous bioactive glass micro- And nanospheres with controlled morphology: Developments, properties and emerging biomedical applications. *Mater Horiz*. 2021;8:300–335. <https://doi.org/10.1039/d0mh01498b>.
12. Kurtuldu F, Mutlu N, Michálek M, Zheng K, Masar M, Liverani L et al. Cerium and gallium containing mesoporous bioactive glass nanoparticles for bone regeneration: Bioactivity, biocompatibility and antibacterial activity. *Mater Sci Eng C*, 2021;124:112050. <https://doi.org/10.1016/j.msec.2021.112050>.
13. Zheng K, Balasubramanian P, Paterson TE, Stein R, MacNeil S, Fiorilli S, et al. Materials Science & Engineering C Ag modified mesoporous bioactive glass nanoparticles for enhanced antibacterial activity in 3D infected skin model. *Mater Sci Eng C*. 2019;103:109764. <https://doi.org/10.1016/j.msec.2019.109764>.
14. Balasubramanian P, Strobel LA, Kneser U, Boccaccini AR. Zinc-containing bioactive glasses for bone regeneration, dental and

- orthopedic applications. *Biomed Glas*. 2015;1:51–69. <https://doi.org/10.1515/bglass-2015-0006>.
15. Molenda M, Kolmas J. The Role of Zinc in Bone Tissue Health and Regeneration — a Review. *Biol Trace Elem Res*. 2023;201:5640–5651. <https://doi.org/10.1007/s12011-023-03631-1>.
  16. Sharifianjazi F, Sharifianjazi M, Irandoost M, Tavamaishvili K, Mohabatkah M, Montazerian M. Advances in Zinc-Containing Bioactive Glasses: A Comprehensive Review. *J Funct Biomater*. 2024;15:258. <https://doi.org/10.3390/jfb15090258>.
  17. Lynch RJM. Zinc in the mouth, its interactions with dental enamel and possible effects on caries; A review of the literature. *Int Dent J*. 2011;61:46–54. <https://doi.org/10.1111/j.1875-595X.2011.00049.x>.
  18. Aziz J, Rahman MT, Vaithilingam RD. Dysregulation of metallothionein and zinc aggravates periodontal diseases. *J Trace Elem Med Biol*. 2021;66:126754. <https://doi.org/10.1016/j.jtemb.2021.126754>.
  19. Esfahanizadeh N, Nourani MR, Bahador A, Akhondi N, Montazeri M. The Anti-biofilm Activity of Nanometric Zinc doped Bioactive Glass against Putative Periodontal Pathogens: An in vitro Study. *Biomed Glas*. 2020;4:95–107. <https://doi.org/10.1515/bglass-2018-0009>.
  20. Zheng K, Boccaccini AR. Sol-gel processing of bioactive glass nanoparticles: A review. *Adv Colloid Interface Sci*. 2017;249:363–373. <https://doi.org/10.1016/j.cis.2017.03.008>.
  21. Vallet-Regí M, Schüth F, Lozano D, Colilla M, Manzano M. Engineering mesoporous silica nanoparticles for drug delivery: where are we after two decades?. *Chem Soc Rev*. 2022;51:5365–5451. <https://doi.org/10.1039/d1cs00659b>.
  22. Neščáková Z, Zheng K, Liverani L, Nawaz Q, Galusková D, Kaňková H, et al. Multifunctional zinc ion doped sol – gel derived mesoporous bioactive glass nanoparticles for biomedical applications. *Bioact Mater*. 2019;4:312–321. <https://doi.org/10.1016/j.bioactmat.2019.10.002>.
  23. Sun H, Zheng K, Zhou T, and Boccaccini AR. Incorporation of zinc into binary SiO<sub>2</sub>–CaO mesoporous bioactive glass nanoparticles enhances anti-inflammatory and osteogenic activities. *Pharmaceutics*. 2021;13:2124. <https://doi.org/10.3390/pharmaceutics13122124>.
  24. Naruphontjirakul P, Li M, Boccaccini AR. Strontium and zinc co-doped mesoporous bioactive glass nanoparticles for potential use in bone tissue engineering applications. *Nanomaterials*. 2024;14:575. <https://doi.org/10.3390/nano14070575>.
  25. Pourshahrestani S, Zeimaran E, Janko C, Alexiou C, Kerpes A, Würz A, et al. The effect of mesoporous bioactive glass nanoparticles incorporating various metallic ions (Cu, Zn, Mn, Te) on wound healing. *Mater Adv*. 2024;5:6630–6647. <https://doi.org/10.1039/d4ma00392f>.
  26. Zhu J, Jiang G, Song G, Liu T, Cao C, Yang Y, et al. Incorporation of ZnO/Bioactive Glass Nanoparticles into Alginate/Chitosan Composite Hydrogels for Wound Closure. *ACS Appl Bio Mater*. 2019;2:5042–5052. <https://doi.org/10.1021/acsabm.9b00727>.
  27. Cai Q, Luo ZS, Pang WQ, Fan YW, Chen XH, Cui FZ. Dilute solution routes to various controllable morphologies of MCM-41 silica with a basic medium. *Chem Mater*. 2001;13:258–263. <https://doi.org/10.1021/cm990661z>.
  28. Li X, Zhang L, Dong X, Liang J, Shi J. Preparation of mesoporous calcium doped silica spheres with narrow size dispersion and their drug loading and degradation behavior. *Microporous Mesoporous Mater*. 2007;102:151–158. <https://doi.org/10.1016/j.micromeso.2006.12.048>.
  29. Tabia Z, El Mabrouk K, Bricha M, Nouneh K. Mesoporous bioactive glass nanoparticles doped with magnesium: drug delivery and acellular in vitro bioactivity. *RSC Adv*. 2019;9:12232–12246. <https://doi.org/10.1039/C9RA01133A>.
  30. Liang Q, Hu Q, Miao G, Yuan B, Chen X. A facile synthesis of novel mesoporous bioactive glass nanoparticles with various morphologies and tunable mesostructure by sacrificial liquid template method. *Mater Lett*. 2015;148:45–49. <https://doi.org/10.1016/j.matlet.2015.01.122>.
  31. Kokubo T, Takadama H. How useful is SBF in predicting in vivo bone bioactivity?. *Biomaterials*. 2006;27:2907–2915. <https://doi.org/10.1016/j.biomaterials.2006.01.017>.
  32. Wajda A, Sitarz M. Structural and microstructural comparison of bioactive melt-derived and gel-derived glasses from CaO–SiO<sub>2</sub> binary system. *Ceram Int*. 2018;44:8856–8863. <https://doi.org/10.1016/j.ceramint.2018.02.070>.
  33. Aguiar H, Serra J, González P, León B. Structural study of sol-gel silicate glasses by IR and Raman spectroscopies. *J Non Cryst Solids*. 2009;355:475–480. <https://doi.org/10.1016/j.jnoncrysol.2009.01.010>.
  34. Fernandes RS, Raimundo IM, Pimentel MF. Revising the synthesis of Stöber silica nanoparticles: A multivariate assessment study on the effects of reaction parameters on the particle size. *Colloids Surf A Physicochem Eng Asp*. 2019;577:1–7. <https://doi.org/10.1016/j.colsurfa.2019.05.053>.
  35. Nidhi N. Synthesis and Characterization of Zinc Oxide Doped Mesoporous Silica SBA-16 and Anti-bacterial Property. *Biosci Biotechnol Res Commun*. 2021;14:194–197. <https://doi.org/10.21786/bbrc/14.9.37>.
  36. Bari A, Bloise N, Fiorilli S, Novajra G, Vallet-Regí M, Bruni G, et al. Copper-containing mesoporous bioactive glass nanoparticles as multifunctional agent for bone regeneration. *Acta Biomater*. 2017;55:493–504. <https://doi.org/10.1016/j.actbio.2017.04.012>.
  37. Wiegand I, Hilpert K, Hancock REW. Agar and broth dilution methods to determine the minimal inhibitory concentration (MIC) of antimicrobial substances. *Nat Protoc*. 2008;3:163–175. <https://doi.org/10.1038/nprot.2007.521>.
  38. Wajda A, Goldmann WH, Detsch R, Boccaccini AR, Sitarz M. Influence of zinc ions on structure, bioactivity, biocompatibility and antibacterial potential of melt-derived and gel-derived glasses from CaO–SiO<sub>2</sub> system. *J Non Cryst Solids*. 2019;511:86–99. <https://doi.org/10.1016/j.jnoncrysol.2018.12.040>.
  39. Başak O, Kurtuldu F, Ilavský J, Vítázková M, Beltrán AM, Muñoz F, et al. Influence of calcium nitrate timing on the structural and textural characteristics of mesoporous SiO<sub>2</sub>–CaO nanoparticles. *Open Ceram*. 2025;23:100807. <https://doi.org/10.1016/j.oceram.2025.100807>.
  40. Taghvaei AH, Mosadeghian F, Mosleh-Shirazi S, Ebrahimi A, Kaňuchová M, Girman V, et al. Fabrication and characterization of novel ZnO-loaded mesoporous bioactive glass nanospheres with enhanced physiochemical properties and biocompatibility for bone tissue engineering. *J Non Cryst Solids*. 2024;626:122781. <https://doi.org/10.1016/j.jnoncrysol.2023.122781>.
  41. Atkinson I. Effect of Sr, Zn, and Ce Substitution on the Properties of Bioactive Glasses. *Am J Biomed Sci Res*. 2020;9:26–29. <https://doi.org/10.34297/ajbsr.2020.10.001467>.
  42. Chiang YD, Lian HY, Leo SY, Wang SG, Yamauchi Y, Wu KCW. Controlling particle size and structural properties of mesoporous silica nanoparticles using the Taguchi method. *J Phys Chem C*. 2011;115:13158–13165. <https://doi.org/10.1021/jp201017e>.
  43. Hu Q, Li Y, Zhao N, Ning C, Chen X. Facile synthesis of hollow mesoporous bioactive glass sub-micron spheres with a tunable cavity size. *Mater Lett*. 2014;134:130–133. <https://doi.org/10.1016/j.matlet.2014.07.041>.
  44. Duan H, Diao J, Zhao N, Ma Y. Synthesis of hollow mesoporous bioactive glass microspheres with tunable shell thickness by hydrothermal-assisted self-transformation method. *Mater Lett*. 2016;167:201–204. <https://doi.org/10.1016/j.matlet.2015.12.162>.
  45. Qiao ZA, Zhang L, Guo M, Liu Y, Huo Q. Synthesis of mesoporous silica nanoparticles via controlled hydrolysis and condensation of silicon alkoxide. *Chem Mater*. 2009;21:3823–3829. <https://doi.org/10.1021/cm901335k>.

46. Liang Q, Hu Q, Miao G, Yuan B, Chen X. A facile synthesis of novel mesoporous bioactive glass nanoparticles with various morphologies and tunable mesostructure by sacrificial liquid template method. *Mater Lett*. 2015;148:45–49. <https://doi.org/10.1016/j.matlet.2015.01.122>.
47. Hench LL. Chronology of Bioactive Glass Development and Clinical Applications. *New J Glas Ceram*. 2013;03:67–73. <https://doi.org/10.4236/njgc.2013.32011>.
48. Zhu Y, Wu C, Ramaswamy Y, Kockrick E, Simon P, Kaskel S, et al. Preparation, characterization and in vitro bioactivity of mesoporous bioactive glasses (MBGs) scaffolds for bone tissue engineering. *Microporous Mesoporous Mater*. 2008;112:494–503. <https://doi.org/10.1016/j.micromeso.2007.10.029>.
49. Aina V, Malavasi G, Fiorio Pla A, Munaron L, Morterra C. Zinc-containing bioactive glasses: Surface reactivity and behaviour towards endothelial cells. *Acta Biomater*. 2009;5:1211–1222. <https://doi.org/10.1016/j.actbio.2008.10.020>.
50. Fandzloch M, Bodylska W, Barszcz B, Trzcińska-Wencel J, Roszek K, Golińska P, et al. Effect of ZnO on sol–gel glass properties toward (bio)application. *Polyhedron*. 2022;223:115952. <https://doi.org/10.1016/j.poly.2022.115952>.
51. De Zheng B, Ye J, Yang YC, Huang YY, Xiao MT. Self-healing polysaccharide-based injectable hydrogels with antibacterial activity for wound healing. *Carbohydr Polym*. 2022;275:118770. <https://doi.org/10.1016/j.carbpol.2021.118770>.
52. Chen YH, Tseng SP, Wu SM, Shih CJ. Structure-dependence of anti-methicillin-resistant staphylococcus aureus (MRSA) activity on ZnO-containing bioglass. *J Alloy Compd*. 2020;848:156487. <https://doi.org/10.1016/j.jallcom.2020.156487>.
53. Shahrabi S, Hesaraki S, Moemeni S, Khorami M. Structural discrepancies and in vitro nanoapatite formation ability of sol-gel derived glasses doped with different bone stimulator ions. *Ceram Int*. 2011;37:2737–2746. <https://doi.org/10.1016/j.ceramint.2011.04.025>.
54. Fortis SP, Batrinou A, Georgatzakou HT, Tsamesidis I, Alvanidis G, Papageorgiou EG, et al. Effect of silica-based mesoporous nanomaterials on human blood cells. *Chem Biol Interact*. 2024;387:110784. <https://doi.org/10.1016/j.cbi.2023.110784>.
55. Everts PA, Malanga GA, Paul RV, Rothenberg JB, Stephens N, Mautner KR. Assessing clinical implications and perspectives of the pathophysiological effects of erythrocytes and plasma free hemoglobin in autologous biologics for use in musculoskeletal regenerative medicine therapies. A review. *Regen Ther*. 2019;11:56–64. <https://doi.org/10.1016/j.reth.2019.03.009>.
56. Pouroutzidou GK, Liverani L, Theocharidou A, Tsamesidis I, Lazaridou M, Christodoulou E, et al. Article synthesis and characterization of mesoporous mg-and Sr-doped nanoparticles for moxifloxacin drug delivery in promising tissue engineering applications. *Int J Mol Sci*. 2021;22:1–25. <https://doi.org/10.3390/ijms22020577>.
57. Mukhopadhyay S, Veroniaina H, Chimombe T, Han L, Zhenghong W, Xiaole Q. Synthesis and compatibility evaluation of versatile mesoporous silica nanoparticles with red blood cells: An overview. *RSC Adv*. 2019;9:35566–35578. <https://doi.org/10.1039/c9ra06127d>.
58. Lin YS, Haynes CL. Impacts of mesoporous silica nanoparticle size, pore ordering, and pore integrity on hemolytic activity. *J Am Chem Soc*. 2010;132:4834–4842. <https://doi.org/10.1021/ja910846q>.
59. Sánchez-Salcedo S, Shruti S, Salinas AJ, Malavasi G, Menabue L, Vallet-Regí M. In vitro antibacterial capacity and cytocompatibility of SiO<sub>2</sub>-CaO-P<sub>2</sub>O<sub>5</sub> meso-macroporous glass scaffolds enriched with ZnO. *J Mater Chem B*. 2014;2:4836–4847. <https://doi.org/10.1039/c4tb00403e>.
60. Sergi R, Bellucci D, Salvatori R, Maisetta G, Batoni G, Cannillo V. Zinc containing bioactive glasses with ultra-high crystallization temperature, good biological performance and antibacterial effects. *Mater Sci Eng C*. 2019;104:109910. <https://doi.org/10.1016/j.msec.2019.109910>.
61. Wang D, Li Q, Xiao C, Wang H, Dong S. “Nanoparticles in Periodontitis Therapy: A Review of the Current Situation,”. *Int J Nanomed*. 2024;19:6857–6893. <https://doi.org/10.2147/IJN.S465089>.
62. Şeker Ş, Elçin AE, Yumak T, Sinağ A, Elçin YM. “In vitro cytotoxicity of hydrothermally synthesized ZnO nanoparticles on human periodontal ligament fibroblast and mouse dermal fibroblast cells. *Toxicol Vitro*. 2014;28:1349–1358. <https://doi.org/10.1016/j.tiv.2014.06.016>.
63. Heras C, Jiménez-Holguín J, Doadrio AL, Vallet-Regí M, Sánchez-Salcedo S, Salinas AJ. Multifunctional antibiotic- and zinc-containing mesoporous bioactive glass scaffolds to fight bone infection. *Acta Biomater*. 2020;114:395–406. <https://doi.org/10.1016/j.actbio.2020.07.044>.